Voltage-Controlled Synthesis of Higher Harmonics in Hybrid Josephson Junction Circuits

L. Banszerus,[1] W. Marshall,[1,2] C. W. Andersson,[1] T. Lindemann,[3,4] M. J. Manfra,[3,4,5,6] C. M. Marcus,[1,2,7] and S. Vaitiekėnas[1]

[1]Center for Quantum Devices, Niels Bohr Institute, University of Copenhagen, 2100 Copenhagen, Denmark
[2]Department of Physics, University of Washington, Seattle, Washington 98195, USA
[3]Department of Physics and Astronomy, Purdue University, West Lafayette, Indiana 47907, USA
[4]Birck Nanotechnology Center, Purdue University, West Lafayette, Indiana 47907, USA
[5]School of Electrical and Computer Engineering, Purdue University, West Lafayette, Indiana 47907, USA
[6]School of Materials Engineering, Purdue University, West Lafayette, Indiana 47907, USA
[7]Materials Science and Engineering, University of Washington, Seattle, Washington 98195, USA

(Received 18 February 2024; revised 9 July 2024; accepted 10 September 2024; published 31 October 2024)

We report measurements of the current-phase relation of two voltage-controlled semiconductor-superconductor hybrid Josephson junctions (JJs) in series. The two hybrid junctions behave similar to a single-mode JJ with effective transparency determined by the ratio of Josephson coupling strengths of the two junctions. Gate-voltage control of Josephson coupling (measured from switching currents) allows tuning of the harmonic content from sinusoidal, for asymmetric tuning, to highly nonsinusoidal, for symmetric tuning. The experimentally observed tunable harmonic content agrees with a model based on two conventional (sinusoidal) JJs in series.

DOI: 10.1103/PhysRevLett.133.186303

Josephson junctions (JJs) support a dissipationless supercurrent, $I(\varphi)$, that depends on the phase difference, φ, between the leads [1]. In conventional superconducting tunnel junctions, sequential coherent transfer of Cooper pairs results in a sinusoidal current-phase relation (CPR) [2]. In contrast, highly transparent JJs allow simultaneous coherent transport of n Cooper pairs, yielding a nonsinusoidal CPR with higher harmonics, $I(\varphi) = \sum_{n=1}^{\infty} A_n \sin(n\varphi)$ [3–6].

Controlling the harmonic content of Josephson elements is crucial for advancing superconducting quantum technologies. Circuits with tunable CPRs allow for simulating the emergence of quantum phases and their transitions [7,8]. Higher harmonics can be used to minimize the charge dispersion of qubit states, thereby enhancing coherence times [9–11], or to engineer double-well Josephson potentials realizing parity-protected qubits with suppressed relaxation and dephasing [12–18]. Furthermore, nonsinusoidal Josephson circuits enable nonlinear superconducting elements [19,20], parametric amplifiers [21–23], and nonreciprocal devices like Josephson diodes [24–27].

One of the main approaches for realizing nonsinusoidal Josephson elements involves circuits comprising multiple sinusoidal JJs. In these circuits, the total phase difference is distributed across the individual JJs, leading to an overall anharmonic behavior [2,28–30]. The resulting CPRs depend on the Josephson energies, E_J, of each junction but are largely independent of microscopic details. One example is the Josephson rhombus with four JJs in a loop [31–33].

An alternative route to higher harmonics is based on individual highly transparent JJs. Such junctions are typically realized in superconductor-normal conductor-superconductor structures with inherently nonsinusoidal CPRs, given by [34]

$$I(\varphi) = \sum_{i=1}^{N} \frac{e\Delta}{2\hbar} \frac{\tau_i \sin(\varphi)}{\sqrt{1 - \tau_i \sin^2(\varphi/2)}}, \tag{1}$$

where Δ is the superconducting gap, τ_i is the transparency of the ith mode, and N is the number of modes. Junctions with high transparency have been observed in various high-mobility platforms, including semiconducting nanowires [35–38], quantum wells [39–42], Van der Waals materials [43–45], and topological insulators [46,47]. These systems allow for voltage-controlled JJs [48–50], whose CPRs depend on device-specific microscopic details affecting the transparencies of each contributing mode and thus the harmonic composition of the CPR.

Here, we investigate hybrid Josephson elements composed of two semiconducting junctions in series with voltage-tunable harmonic content. Previous theory showed that CPR of two sinusoidal JJs in series can be described by Eq. (1); see Ref. [27]. In this case, Δ is replaced by the sum of the Josephson energies, $\sigma = E_{J1} + E_{J2}$, and the effective transparency is given by $\tau = 4\rho/(1+\rho)^2$, where $\rho = E_{J1}/E_{J2}$. We experimentally tune ρ by changing the ratio of the two-junction switching currents, I_{SW1}/I_{SW2}, and demonstrate a controlled transition from sinusoidal to

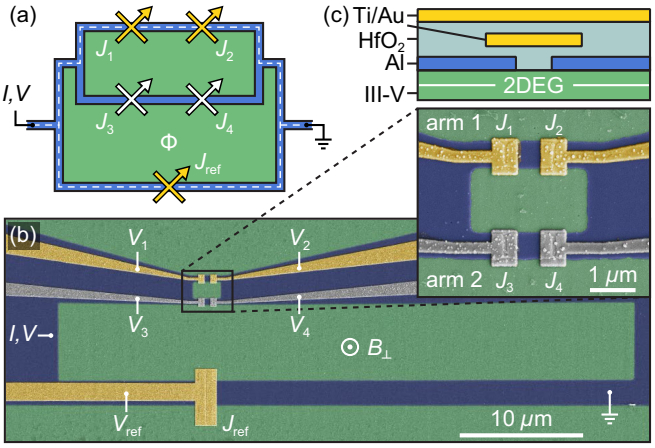

FIG. 1. (a) Schematic of the measured device comprising two parallel arms, each with two voltage-tunable JJs in series, embedded in a loop with a reference junction for current-phase relation measurements. (b) Color-enhanced scanning electron micrograph of a reference device, taken before the deposition of the global top gate. The exposed semiconductor is green, and the epitaxial Al is blue. Colorized gate configuration highlights the setup for measuring the CPR of arm 1, with conducting (depleted) JJs under yellow (gray) gates. The inset shows an enlargement of the two arms of the device. (c) Schematic cross section of a junction showing the dual-gate configuration. The local gate (first layer) tunes the Josephson coupling, while the global gate (second layer, kept at −1.3 V throughout the experiment) depletes the surrounding 2DEG.

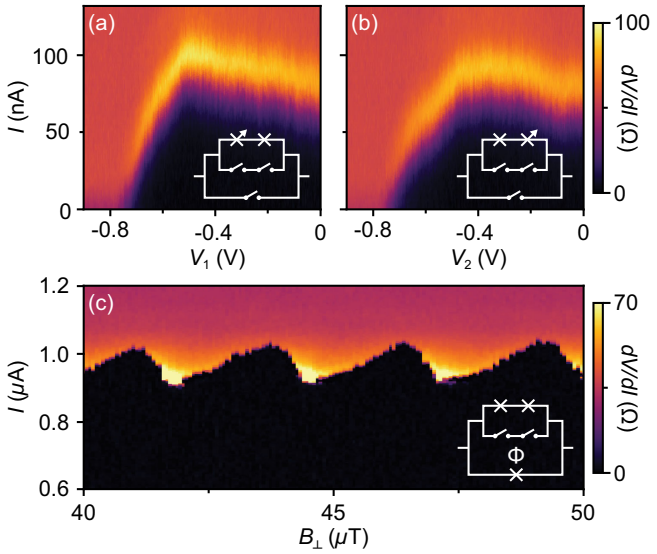

FIG. 2. (a) Differential resistance, dV/dI, as a function of current bias, I, and J_1 gate voltage, V_1, measured for arm 1 with open J_2 ($V_2 = 0$). Arm 2 and J_{ref} were pinched off ($V_4 = -1$ V, $V_{ref} = -1.5$ V). (b) Similar to (a) but taken as a function of V_2, with $V_1 = 0$. For both junctions, the switching current is maximal around $V_1, V_2 = -0.5$ V and is fully suppressed at −0.8 V. (c) Resistance as a function of I and flux-threading perpendicular magnetic field, $B_\perp$, measured with arm 1 and J_{ref} open, but arm 2 isolated. The skewed oscillations in the switching current suggest a highly nonsinusoidal current-phase relation.

highly nonsinusoidal CPR, with substantial contributions from the first four harmonics. Realizing the same harmonic content in a single JJ would require a mode with an intrinsic transparency $\tau_{int} > 0.95$, which remains challenging to achieve in a controlled manner due to disorder-induced fluctuations in E_J [51,52].

Devices were fabricated using an InAs two-dimensional electron gas (2DEG) heterostructure, proximitized by an epitaxial Al layer. The Al film was lithographically patterned to form two parallel arms, each with two JJs in series, denoted J_1, J_2 in arm 1, and J_3, J_4 in arm 2. Both arms were embedded in a loop with a reference junction, J_{ref}, designed to have a much higher critical current compared to the other JJs; see Figs. 1(a) and 1(b). Individual junction Ti/Au top gates were metallized after atomic layer deposition of HfOx, allowing for independent electrostatic control. A second set of HfOx dielectric and a global Ti/Au gate were fabricated to deplete the surrounding 2DEG. The complete device stack is illustrated in Fig. 1(c). The two arms showed similar results. We report representative data from both devices in the main text and present supporting data in the Supplemental Material [53]. Measurements were performed in a dilution refrigerator with a three-axis vector magnet and base temperature of 20 mK using standard ac lock-in techniques in a four-terminal configuration. Further details on wafer structure, sample fabrication, and measurements are given in the Supplemental Material [53].

We begin by investigating the supercurrent transport through arm 1, while keeping arm 2 and J_{ref} pinched off. Differential resistance, dV/dI, as a function of current bias, I, and gate voltage V_1 [Fig. 2(a)] or V_2 [Fig. 2(b)] shows switching current, I_{SW}, that initially increases with decreasing gate voltage, reaching nearly 100 nA at $V_1, V_2 \sim -0.5$ V, but then gets fully suppressed at around −0.8 V. A comparison of the switching and retrapping currents shows no hysteresis, indicating overdamped junctions [53]. To measure the CPR of arm 1, we open J_{ref} by setting $V_{ref} = 0$ and apply a flux-threading perpendicular magnetic field, $B_\perp$. The measured dV/dI reveals a periodic switching current of ∼1 μA, modulated by nonsinusoidal oscillations with an amplitude of ∼100 nA and a period of ∼2.5 μT [see Fig. 2(c)]. We attribute the large background I_{SW} to J_{ref} and the oscillatory component, ΔI_{SW}, to the flux-induced modulation of phase difference across the two JJs in arm 1.

To better understand the origin of the nonsinusoidal CPR, we model the measured Josephson elements as two sinusoidal junctions in series, following Ref. [27]. The total energy of the system is $E_{tot} = E_{J1}[1 - \cos(\varphi_1)] + E_{J2}[1 - \cos(\varphi_2)]$, with the total phase differences across both JJs defined by the external phase bias $\varphi = \varphi_1 + \varphi_2$ [2,28]. Minimizing the total energy under this boundary

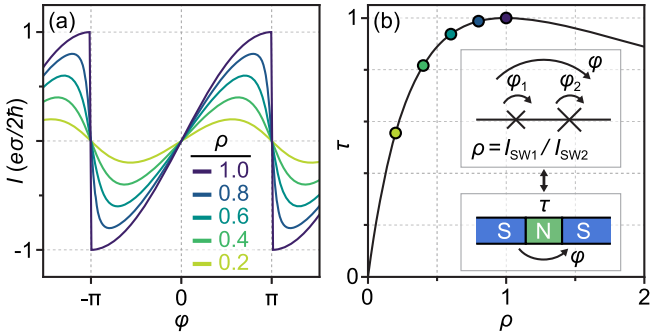

FIG. 3. (a) Theoretical current-phase relation of two sinusoidal Josephson junctions in series [Eq. (2)] for various ratios of the Josephson energies $\rho = E_{J1}/E_{J2}$. The relation evolves from sinusoidal to highly nonsinusoidal as ρ approaches 1. (b) Mapping between ρ and the transparency of a single-mode junction, τ.

condition yields the phase-dependent ground-state energy $E_0(\varphi) = -\sigma\sqrt{1-[4\rho/(1+\rho)^2]\sin^2(\varphi/2)}$. The corresponding CPR is given by

$$I(\varphi) = \frac{2e}{\hbar}\frac{\partial E_0}{\partial \varphi} = \frac{e\sigma}{2\hbar}\frac{4\rho}{(1+\rho)^2}\frac{\sin(\varphi)}{\sqrt{1-\frac{4\rho}{(1+\rho)^2}\sin^2(\varphi/2)}}. \quad (2)$$

We note that Eq. (2) has the same functional form as the expression for CPR of a transparent single-mode junction described by Eq. (1), where σ acts as Δ and the term $4\rho/(1+\rho)^2$ serves as τ. The symmetrized case ($\rho = 1$) corresponds to one fully transmissive mode ($\tau = 1$), with highly nonsinusoidal CPR [Fig. 3(a)]. Away from the symmetry point, the effective transparency decreases but remains $\gtrsim 0.9$ for ρ between 0.5 to 2 [Fig. 3(b)]. In the limit of $\rho \gg 1$ and $\rho \ll 1$, the CPR of the double JJ approaches the CPR of the single JJ with the smaller E_J. We find that a purely sinusoidal CPR of the individual JJs is a good approximation as long as $4\rho/(1+\rho)^2$ is larger than the intrinsic transparencies of the JJs. The case of nonsinusoidal JJs is studied numerically in the Supplemental Material [53].

To test the model experimentally, we investigate the CPR of arm 2 for different junction configurations (analogous data from arm 1 is presented in the Supplemental Material [53]). In the desymmetrized case, with highly conductive J_3 and nearly depleted J_4 ($V_3 = 0$, $V_4 = -0.76$ V), the switching current exhibits roughly sinusoidal modulations; see Fig. 4(a). We attribute the additional fine modulations in the switching current to the switching statistics of the superconducting circuit. For a quantitative analysis, we extract the oscillatory component of the switching current, ΔI_{SW}, corresponding to the CPR of arm 2 [Fig. 4(b)]. Fitting these data to Eq. (2) yields $\rho = 0.02 \pm 0.02$ [orange curve in Fig. 4(b)]. Taking a fast Fourier transform of the

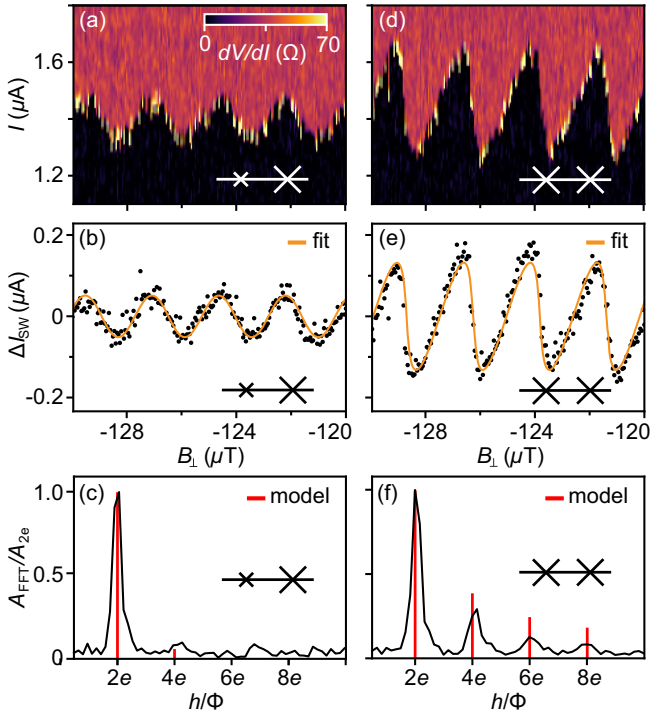

FIG. 4. (a) Differential resistance, dV/dI, as a function of current bias, I, and perpendicular magnetic field, $B_\perp$, for arm 2 in the desymmetrized regime ($V_3 = 0$, $V_4 = -0.76$ V), with open J_{ref} ($V_{ref} = 0$) but pinched-off arm 1 ($V_1 = -1$ V, $V_2 = -1$ V). (b) Switching-current oscillations, ΔI_{SW}, inferred from data in (a). Fit to Eq. (2) yields $\rho = 0.02$, corresponding to an effective $\tau = 0.09$. (c) Fast Fourier transform amplitude of ΔI_{SW} from (b), in the range of $B_\perp = -140$ to -110 μT. The red bars indicate the expected amplitude of the harmonics calculated from the ratio of the switching currents of J_3 and J_4. (d)–(f) Same as (a)–(c) but for the symmetrized case with $V_3 = 0$ and $V_4 = -0.56$ V. The fit to Eq. (2) in (e) yields $\rho = 0.63$, corresponding to an effective $\tau = 0.95$.

measured ΔI_{SW} reveals the harmonic content of the CPR, characterized by a prominent peak at the first harmonic ($2e$) and nearly absent higher-order components [Fig. 4(c)]. The observed Fourier spectrum agrees well with the expected harmonic amplitudes [red bars in Fig. 4(c)], determined by the independently measured ratio of the switching currents, $\rho = I_{SW3}/I_{SW4} = 0.08 \pm 0.07$, with the confidence interval based on the width of I_{SW} features.

In the symmetrized scenario, with both J_3 and J_4 open ($V_3 = 0$, $V_4 = -0.56$ V), the oscillatory component of I_{SW} displays a highly nonsinusoidal, sawtoothlike behavior; see Fig. 4(d). A fit of Eq. (2) to the extracted ΔI_{SW} yields $\rho = 0.63 \pm 0.01$ [Fig. 4(e)]. Mapping this value to a single-mode JJ corresponds to a transparency of $\tau = 0.95 \pm 0.05$. The Fourier transform of ΔI_{SW} reveals considerable contributions from the first four harmonics ($2e$, $4e$, $6e$, and $8e$), in a good agreement with the expected harmonic amplitudes based on independently measured, $\rho = I_{SW3}/I_{SW4} = 0.82 \pm 0.02$; see Fig. 4(f). Arm 1 shows

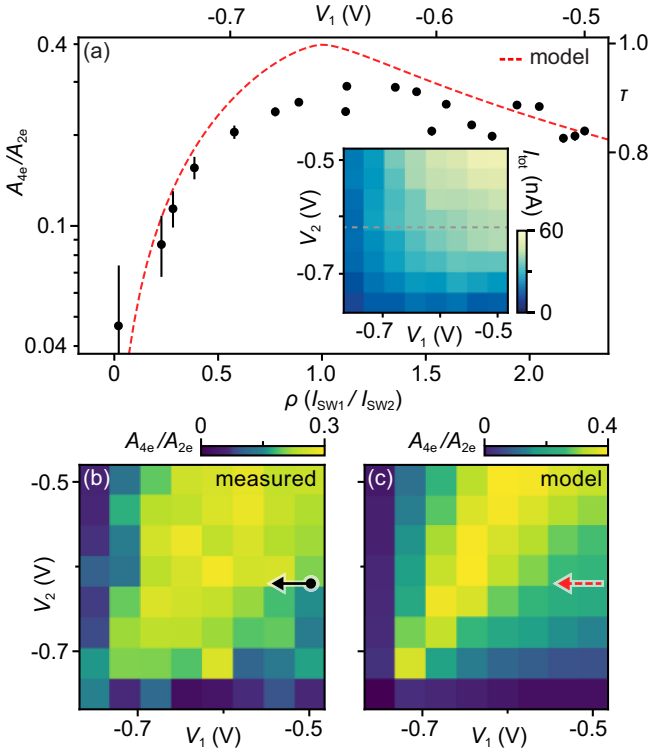

FIG. 5. (a) Ratio of second to first harmonic amplitudes, A_{4e}/A_{2e}, determined from fits to CPR, plotted against independently measured $\rho = I_{SW1}/I_{SW2}$ for arm 1. Error bars indicate uncertainties in the fits to Eq. (2). Data were taken with varying V_1 between −0.75 and −0.5 V and fixed $V_2 = -0.62$ V. The dashed red curve is the expected A_{4e}/A_{2e} based on the measured switching currents. Inset: gate-voltage evolution of the total switching current, I_{tot}, of arm 1 determined from fits to CPRs. (b) Measured and (c) expected A_{4e}/A_{2e} ratio as a function of V_1 and V_2.

similar behavior for symmetrized and desymmetrized configurations [53].

Finally, we demonstrate experimentally a deterministic control of harmonic content by investigating the CPR of arm 1 as a function of V_1, keeping V_2 fixed. To quantify the nonsinusoidal nature of the CPR, we Fourier transform the measured ΔI_{SW} and study the ratio between the second and first harmonic, A_{4e}/A_{2e}. Figure 5(a) displays a parametric plot of A_{4e}/A_{2e} against the independently measured $\rho = I_{SW1}/I_{SW2}$, with V_1 varying from −0.75 to −0.5 V and V_2 set to −0.62 V. The measured A_{4e}/A_{2e} follows the expected behavior based on Eq. (2) [dashed red curve in Fig. 5(a)], reaching a value of $A_{4e}/A_{2e} \sim 0.3$ around $\rho = 1$, lower than the theoretical maximum of 0.4. Arm 2 shows a qualitatively similar behavior, with a weaker ρ dependence of A_{4e}/A_{2e}, which we attribute to a non-negligible intrinsic junction transparency (see Supplemental Material [53]).

It is unlikely that the observed discrepancy between measured and expected A_{4e}/A_{2e} near $\rho = 1$ is due to thermal smearing, as $k_B T \sim 2$ μeV is about 2 orders of magnitude smaller than the Josephson energy $\hbar \Delta I_{SW}/2e \sim 0.2$ meV. To examine the self-biasing as a possible explanation, we estimate the kinetic inductance of the superconducting loop to be $L_K \sim 300$ pH [54]. This indicates that the nonlinearities between the total and external fluxes, $\Phi = \Phi_{ext} - L_K \Delta I_{SW}(\varphi)$, can amount to ∼1% of the superconducting flux quantum, Φ_0 [39]. The estimated geometric inductance of the loop, $L_G \sim 40$ pH, is considerably smaller and thus negligible compared to L_K. Instead, we suspect that the measured values of A_{4e}/A_{2e} are limited by flux noise originating from the relatively large loop area and wide leads, resulting in a smearing of the CPR.

A map of A_{4e}/A_{2e}, measured as a function of V_1 and V_2, reveals that the ratio of the first two harmonics is maximal along the diagonal where $V_1 \sim V_2$, with the stability range expanding at less negative voltage; see Fig. 5(b). The data is in good qualitative agreement with the expected A_{4e}/A_{2e} based on Eq. (2) and the independently measured $I_{SW1}(V_1)$ and $I_{SW2}(V_2)$ [Fig. 5(c)]. We note that away from pinch-off, A_{4e}/A_{2e} remains approximately constant for symmetrized arm 1, whereas its total switching current, $I_{tot} = \sigma\rho/\Phi_0(1+\rho)^2$, continues increasing with the gate voltages; see the inset in Fig. 5(a). This highlights the unique feature of the investigated hybrid Josephson elements, namely the independent voltage control of the harmonics content (characterized by A_{4e}/A_{2e}) and the effective Josephson energy (represented by I_{tot}).

In summary, we have demonstrated an experimental method to deterministically synthesize tunable and highly nonsinusoidal Josephson elements consisting of two junctions in series, implemented in an InAs/Al hybrid heterostructure. The approach combines the advantages of voltage control and resilience against microscopic device-to-device variations. By controlling the switching current of each junction, the effective Josephson energy and harmonic content of the Josephson element can be tuned independently. Our findings pave a new way for the realization of alternative superconducting qubits with improved coherence times, such as charge-insensitive qubits based on high effective transmission [9,10] or parity-protected qubits in a $\cos(2\varphi)$ potential [16,18]. The *in situ* tunability of the Josephson potential enables advanced qubits operation schemes [55], tunable parametric amplifiers [21–23], nonlinear Josephson circuits [56–58], and nonreciprocal Josephson diodes [25,27,59].

Acknowledgments—We thank A. C. C. Drachmann and S. Sasmal for assistance with the device fabrication and M. Kjaergaard for discussions. We acknowledge support from research grants (Projects No. 43951, No. 50334, and No. 53097) from VILLUM FONDEN, the Danish National Research Foundation, and the European Research Council (Grant Agreement No. 856526).

[1] B. D. Josephson, Phys. Lett. **1**, 251 (1962).
[2] A. A. Golubov, M. Yu. Kupriyanov, and E. Il'ichev, Rev. Mod. Phys. **76**, 411 (2004).

[3] C. Ishii, Prog. Theor. Phys. **44**, 1525 (1970).
[4] K. K. Likharev, Rev. Mod. Phys. **51**, 101 (1979).
[5] M. L. Della Rocca, M. Chauvin, B. Huard, H. Pothier, D. Esteve, and C. Urbina, Phys. Rev. Lett. **99**, 127005 (2007).
[6] A. Murani, A. Kasumov, S. Sengupta, Y. A. Kasumov, V. T. Volkov, I. I. Khodos, F. Brisset, R. Delagrange, A. Chepelianskii, R. Deblock, H. Bouchiat, and S. Guéron, Nat. Commun. **8**, 15941 (2017).
[7] D. Kuzmanovski, R. S. Souto, P. J. Wong, and A. V. Balatsky, arXiv:2312.03456.
[8] L. Maffi, N. Tausendpfund, M. Rizzi, and M. Burrello, Phys. Rev. Lett. **132**, 226502 (2024).
[9] A. Kringhøj, B. van Heck, T. W. Larsen, O. Erlandsson, D. Sabonis, P. Krogstrup, L. Casparis, K. D. Petersson, and C. M. Marcus, Phys. Rev. Lett. **124**, 246803 (2020).
[10] A. Bargerbos, W. Uilhoorn, C.-K. Yang, P. Krogstrup, L. P. Kouwenhoven, G. de Lange, B. van Heck, and A. Kou, Phys. Rev. Lett. **124**, 246802 (2020).
[11] D. Willsch *et al.*, Nat. Phys. **20**, 815 (2024).
[12] L. B. Ioffe and M. V. Feigel'man, Phys. Rev. B **66**, 224503 (2002).
[13] B. Douçot and L. B. Ioffe, Rep. Prog. Phys. **75**, 072001 (2012).
[14] M. T. Bell, J. Paramanandam, L. B. Ioffe, and M. E. Gershenson, Phys. Rev. Lett. **112**, 167001 (2014).
[15] G. de Lange, B. van Heck, A. Bruno, D. J. van Woerkom, A. Geresdi, S. R. Plissard, E. P. A. M. Bakkers, A. R. Akhmerov, and L. DiCarlo, Phys. Rev. Lett. **115**, 127002 (2015).
[16] W. C. Smith, A. Kou, X. Xiao, U. Vool, and M. H. Devoret, npj Quantum Inf. **6**, 8 (2020).
[17] A. Gyenis, A. Di Paolo, J. Koch, A. Blais, A. A. Houck, and D. I. Schuster, PRX Quantum **2**, 030101 (2021).
[18] C. Schrade, C. M. Marcus, and A. Gyenis, PRX Quantum **3**, 030303 (2022).
[19] D. Hover, Y.-F. Chen, G. J. Ribeill, S. Zhu, S. Sendelbach, and R. McDermott, Appl. Phys. Lett. **100**, 063503 (2012).
[20] N. E. Frattini, U. Vool, S. Shankar, A. Narla, K. M. Sliwa, and M. H. Devoret, Appl. Phys. Lett. **110**, 222603 (2017).
[21] B. Abdo, K. Sliwa, L. Frunzio, and M. Devoret, Phys. Rev. X **3**, 031001 (2013).
[22] V. V. Sivak, S. Shankar, G. Liu, J. Aumentado, and M. H. Devoret, Phys. Rev. Appl. **13**, 024014 (2020).
[23] C. Schrade and V. Fatemi, Phys. Rev. Appl. **21**, 064029 (2023).
[24] C. Baumgartner, L. Fuchs, A. Costa, S. Reinhardt, S. Gronin, G. C. Gardner, T. Lindemann, M. J. Manfra, P. E. Faria Junior, D. Kochan, J. Fabian, N. Paradiso, and C. Strunk, Nat. Nanotechnol. **17**, 39 (2022).
[25] R. S. Souto, M. Leijnse, and C. Schrade, Phys. Rev. Lett. **129**, 267702 (2022).
[26] C. Ciaccia, R. Haller, A. C. C. Drachmann, T. Lindemann, M. J. Manfra, C. Schrade, and C. Schönenberger, Phys. Rev. Res. **5**, 033131 (2023).
[27] A. M. Bozkurt, J. Brookman, V. Fatemi, and A. R. Akhmerov, SciPost Phys. **15**, 204 (2023).
[28] Yu. S. Barash, Phys. Rev. B **97**, 224509 (2018).
[29] M. Coraiola, D. Z. Haxell, D. Sabonis, H. Weisbrich, A. E. Svetogorov, M. Hinderling, S. C. t. Kate, E. Cheah, F. Krizek, R. Schott, W. Wegscheider, J. C. Cuevas, W. Belzig, and F. Nichele, Nat. Commun. **14**, 6784 (2023).
[30] S. Matsuo, T. Imoto, T. Yokoyama, Y. Sato, T. Lindemann, S. Gronin, G. C. Gardner, M. J. Manfra, and S. Tarucha, Sci. Adv. **9**, adj3698 (2023).
[31] B. Douçot and J. Vidal, Phys. Rev. Lett. **88**, 227005 (2002).
[32] I. M. Pop, K. Hasselbach, O. Buisson, W. Guichard, B. Pannetier, and I. Protopopov, Phys. Rev. B **78**, 104504 (2008).
[33] S. Gladchenko, D. Olaya, E. Dupont-Ferrier, B. Douçot, L. B. Ioffe, and M. E. Gershenson, Nat. Phys. **5**, 48 (2009).
[34] C. W. J. Beenakker, Phys. Rev. Lett. **67**, 3836 (1991).
[35] D. J. v. Woerkom, A. Proutski, B. v. Heck, D. Bouman, J. I. Väyrynen, L. I. Glazman, P. Krogstrup, J. Nygård, L. P. Kouwenhoven, and A. Geresdi, Nat. Phys. **13**, 876 (2017).
[36] E. M. Spanton, M. Deng, S. Vaitiekėnas, P. Krogstrup, J. Nygård, C. M. Marcus, and K. A. Moler, Nat. Phys. **13**, 1177 (2017).
[37] T. W. Larsen, M. E. Gershenson, L. Casparis, A. Kringhøj, N. J. Pearson, R. P. G. McNeil, F. Kuemmeth, P. Krogstrup, K. D. Petersson, and C. M. Marcus, Phys. Rev. Lett. **125**, 056801 (2020).
[38] K. Ueda, S. Matsuo, H. Kamata, Y. Sato, Y. Takeshige, K. Li, L. Samuelson, H. Xu, and S. Tarucha, Phys. Rev. Res. **2**, 033435 (2020).
[39] F. Nichele, E. Portolés, A. Fornieri, A. M. Whiticar, A. C. C. Drachmann, S. Gronin, T. Wang, G. C. Gardner, C. Thomas, A. T. Hatke, M. J. Manfra, and C. M. Marcus, Phys. Rev. Lett. **124**, 226801 (2020).
[40] C. Ciaccia, R. Haller, A. C. C. Drachmann, T. Lindemann, M. J. Manfra, C. Schrade, and C. Schönenberger, Commun. Phys. **7**, 41 (2024).
[41] M. Valentini, O. Sagi, L. Baghumyan, T. d. Gijsel, J. Jung, S. Calcaterra, A. Ballabio, J. A. Servin, K. Aggarwal, M. Janik, T. Adletzberger, R. S. Souto, M. Leijnse, J. Danon, C. Schrade, E. Bakkers, D. Chrastina, G. Isella, and G. Katsaros, Nat. Commun. **15**, 169 (2024).
[42] A. Leblanc, C. Tangchingchai, Z. S. Momtaz, E. Kiyooka, J.-M. Hartmann, G. T. Fernandez-Bada, Z. Scherübl, B. Brun, V. Schmitt, S. Zihlmann, R. Maurand, É. Dumur, S. De Franceschi, and F. Lefloch, Phys. Rev. Res. **6**, 033281 (2024).
[43] C. D. English, D. R. Hamilton, C. Chialvo, I. C. Moraru, N. Mason, and D. J. Van Harlingen, Phys. Rev. B **94**, 115435 (2016).
[44] G. Nanda, J. L. Aguilera-Servin, P. Rakyta, A. Kormányos, R. Kleiner, D. Koelle, K. Watanabe, T. Taniguchi, L. M. K. Vandersypen, and S. Goswami, Nano Lett. **17**, 3396 (2017).
[45] E. Portolés, S. Iwakiri, G. Zheng, P. Rickhaus, T. Taniguchi, K. Watanabe, T. Ihn, K. Ensslin, and F. K. de Vries, Nat. Nanotechnol. **17**, 1159 (2022).
[46] I. Sochnikov, L. Maier, C. A. Watson, J. R. Kirtley, C. Gould, G. Tkachov, E. M. Hankiewicz, C. Brüne, H. Buhmann, L. W. Molenkamp, and K. A. Moler, Phys. Rev. Lett. **114**, 066801 (2015).
[47] S. Ghatak, O. Breunig, F. Yang, Z. Wang, A. A. Taskin, and Y. Ando, Nano Lett. **18**, 5124 (2018).

[48] J. A. v. Dam, Y. V. Nazarov, E. P. A. M. Bakkers, S. D. Franceschi, and L. P. Kouwenhoven, Nature (London) **442**, 667 (2006).
[49] J.-P. Cleuziou, W. Wernsdorfer, V. Bouchiat, T. Ondarçuhu, and M. Monthioux, Nat. Nanotechnol. **1**, 53 (2006).
[50] M. Kjaergaard, H. J. Suominen, M. P. Nowak, A. R. Akhmerov, J. Shabani, C. J. Palmstrøm, F. Nichele, and C. M. Marcus, Phys. Rev. Appl. **7**, 034029 (2017).
[51] M. F. Goffman, C. Urbina, H. Pothier, J. Nygård, C. M. Marcus, and P. Krogstrup, New J. Phys. **19**, 092002 (2017).
[52] S. Hart, Z. Cui, G. Ménard, M. Deng, A. E. Antipov, R. M. Lutchyn, P. Krogstrup, C. M. Marcus, and K. A. Moler, Phys. Rev. B **100**, 064523 (2019).
[53] See Supplemental Material at http://link.aps.org/supplemental/10.1103/PhysRevLett.133.186303 for sample preparation and measurement details, theoretical model description, and additional data.
[54] A. J. Annunziata, D. F. Santavicca, L. Frunzio, G. Catelani, M. J. Rooks, A. Frydman, and D. E. Prober, Nanotechnology **21**, 445202 (2010).
[55] S. Krøjer, A. E. Dahl, K. S. Christensen, M. Kjaergaard, and K. Flensberg, Phys. Rev. Res. **6**, 023064 (2024).
[56] J.-D. Pillet, V. Benzoni, J. Griesmar, J.-L. Smirr, and C. O. Girit, Nano Lett. **19**, 7138 (2019).
[57] A. Melo, V. Fatemi, and A. R. Akhmerov, SciPost Phys. **12**, 017 (2022).
[58] F. J. Matute-Cañadas, L. Tosi, and A. L. Yeyati, PRX Quantum **5**, 020340 (2024).
[59] Y. Zhang, Y. Gu, P. Li, J. Hu, and K. Jiang, Phys. Rev. X **12**, 041013 (2022).